Impact of deforestation and climate on the Amazon Basin's above-ground biomass during 1993-2012

Impact of deforestation and climate on the Amazon Basin's above-ground biomass during 1993-2012

Jean-François Exbrayat[1]*, Yi Y. Liu[2,3] and Mathew Williams[1]

[1] School of GeoSciences and National Centre for Earth Observation, University of Edinburgh, Edinburgh UK

[2] School of Geography and Remote Sensing, Nanjing University of Information Science and Technology, Nanjing, China

[3] ARC Centre of Excellence for Climate System Science and Climate Change Research Centre, University of New South Wales, Sydney, NSW, Australia

*correspondence to: j.exbrayat@ed.ac.uk

Last edited: 26 October 2017

Abstract

Since the 1960s, large-scale deforestation in the Amazon Basin has contributed to rising global CO_2 concentrations and to climate change. Recent advances in satellite observations enable estimates of gross losses of above-ground biomass (AGB) stocks due to deforestation. However, because of simultaneous regrowth, the net contribution of deforestation emissions to rising atmospheric CO_2 concentrations is poorly quantified. Climate change may also reduce the potential for forest regeneration in previously disturbed regions. Here, we address these points of uncertainty with a machine-learning approach that combines satellite observations of AGB with climate data across the Amazon Basin to reconstruct annual maps of potential AGB during 1993-2012, the above-ground C storage potential of the undisturbed landscape. We derive a 2.2 Pg C loss of AGB over the study period, and, for the regions where these losses occur, we estimate a 0.7 Pg C reduction in potential AGB. Thus, climate change has led to a decline of ~1/3 in the capacity of these disturbed forests to recover and recapture the C lost in disturbances during 1993-2012. Our approach further shows that annual variations in land use change mask the natural relationship between the El Niño/Southern Oscillation and AGB stocks in disturbed regions.

The terrestrial carbon sink helps offset about 25% of anthropogenic emissions of fossil-fuel responsible for climate change[1,2]. While tropical forests are a major contributor to this sink, recent large-scale deforestation has weakened the capacity of the Amazonian forest to remain a long-term carbon store. The extent of land cover change in the Amazon Basin can now be quantified with some degrees of confidence using satellite-based observations[3]. Merging these observations with maps[4,5] of Aboveground Biomass Carbon (AGB) provides a baseline estimation of gross losses from deforestation[6]. However, corresponding emissions may be partially compensated by regrowth in previously cleared areas[1] while climate change, and extremes in particular, may alter the capacity of Amazonian forests to sequester C[7]. Therefore, estimates of the long-term net impact of large-scale deforestation and degradation on the land carbon sink, and its potential for recovery, are challenging to establish.

A way to address these problems is to study the deviation of current AGB stocks from potential stocks, to determine and separate the human-induced and climate-induced biomass deficits. These potential stocks are those that would exist under current climate if previous large-scale deforestation and degradation had not occurred (potential AGB further noted as AGB_{pot}[8]; see Methods). AGB_{pot} can also be considered as a measure of local suitability for long-term carbon storage to inform reforestation and afforestation mitigation strategies. While it is not a directly measurable quantity, AGB_{pot} is comparable to carbon stocks predicted by terrestrial ecosystem models that omit land use and land cover change activities[8] (such as those participating in the Intersectoral Impact Model Intercomparison Project, ISI-MIP[9-11]).

In a previous study[8], maps of AGB_{pot} have been reconstructed over the Amazon Basin based on the relationship between climate[12] and maps of observed AGB in the tropics[4,5] (AGB_{obs}) inside Intact Forest Landscapes[13] (IFL). This study estimated a current human-driven AGB deficit ($AGB_{def} = AGB_{pot} - AGB_{obs}$) ranging from 7.3 to 8 Pg C, or 11.6-12.2% of the basin-wide AGB_{pot}. However, this previous approach relied on AGB_{obs} derived from data amalgamated over several years, which prevented any analysis of the evolution of AGB_{def}. Indeed, AGB_{def} continuously evolves through time as it is the difference between AGB_{pot}, which is only driven by climate and atmospheric CO_2

concentrations, and AGB_{obs} which is driven by land use activities as well as climate and atmospheric CO_2 concentrations. For example, anthropogenic activities such as deforestation (regrowth) may lead to a decrease (increase) in AGB_{obs} stocks, resulting in positive (negative) trend in AGB_{def}. Meanwhile, the CO_2-fertilization effect may lead to a greater potential for forest regeneration (i.e. greater AGB_{pot}) as recent findings indicates it is the main driver of a global greening of the land surface[14]. However, locally changing climate conditions may lead to a reduction of the resilience of tropical forests and a transition toward less densely vegetated savannah landscapes[15]. There is a projected risk of Amazon die-back[7] due to climate change, albeit with large uncertainty on its occurrence and severity[16]. It would reduce the potential for biomass recovery associated with reforestation by the end of the 21st century. Therefore, it is important to estimate the resilience of AGB_{pot} to climate change to design efficient climate mitigation strategies based on reforestation.

In this study, we build on a previous approach[8] (see Methods) to address the evolution of AGB_{pot}, and hence AGB_{def}, using a new dataset[17] that provides annual estimates of AGB_{obs} from 1993 to 2012 at a 0.25° spatial resolution. By doing so, we aim to answer the following questions:

- How did AGB_{def} evolve in disturbed regions of the Amazon Basin over these two decades?
- Can we apportion this evolution to climate conditions affecting AGB_{pot} versus human activities reducing AGB_{obs}?
- Would reforestation-based mitigation strategies be resilient to climate change in previously cleared regions of the Amazon Basin?

Results

We estimate a change in AGB_{obs} from 26.3 Pg C (with a 4.1 Pg C confidence range) in 1993 to 24.1 Pg C (with a 3.9 Pg C confidence range) in 2012, or a 2.2 Pg C (with a 0.2 Pg C confidence range) loss in regions of the Amazon basin which are not IFL. Using the machine-learning approach we derive a reduction of AGB_{pot} from 32.1 Pg C (with a 4.0 Pg C confidence range) in 1993 to 31.4 (with a 3.9 Pg C confidence range) in 2012 in the same regions. Comparing the evolution of AGB_{obs} and

89 AGB_{pot} results in a human-driven increase in AGB_{def} from 18.0% (AGB_{def}/AGB_{pot}) in 1993 (with a
90 2.3% confidence range) to 23.3% in 2012 (with a 2.7 % confidence range). Overall, ~1.5 Pg C of the
91 ~7.3 Pg C mean AGB_{def} in 2012 was generated by combined anthropogenic activities and climate
92 patterns since 1993 (Table 1). The evolution of AGB_{def} is strongly linear during 1993-2005 (r = 0.99;
93 $p << 0.001$) before plateauing from 2005 onwards with no significant trend (Figure 1). The
94 stabilisation of AGB_{def} after 2005 is associated to a reduction of AGB_{obs} stocks from 0.17 Pg C y^{-1}
95 (with a 6% relative uncertainty) to 0.04 Pg C y^{-1} (with a 14% relative uncertainty) before and after
96 2005 respectively (Figure 2). It corresponds to a reduction in deforestation rates over the Brazilian
97 Amazon seen in data from INPE (Figure S1 in the Supplementary Information; $r = 0.97$; $p << 0.001$)
98 while the smooth decreases of AGB_{pot} throughout the study period indicates a long-term negative
99 impact of climate on the regeneration potential of disturbed regions (Figure 2).

100 The increase in AGB_{def} is heterogeneously distributed across disturbed areas of the basin (Figure 3).
101 While the spatial distributions of AGB_{def} are significantly correlated (r = 0.89; $p << 0.001$) in 1993
102 (Figure 3a) and 2012 (Figure 3b), AGB_{def} increased by more than 50 Mg C ha^{-1} in some parts of the
103 Brazilian arc of deforestation (between 10°S and 15°S; Figure 3c) and in central Bolivia (south of
104 15°S; Figure 3c). We note a reduction in AGB_{def}, i.e. a recovery of AGB_{obs} stocks toward AGB_{pot}, in
105 the south-eastern edge of the basin, and to a lesser extent in northern Brazil. This recovery indicates
106 that non-primary vegetation, mostly rangeland in these regions, may have built up biomass stocks
107 from 1993 to 2012. Over the period 1993-2012, local increases in AGB_{def} can be explained by the
108 erosion of primary land (Figure 4). Conversely, local recovery of stocks associated to decreases in
109 AGB_{def} corresponds to regions where the fraction of primary land was already low in 1993. This
110 pattern indicates a recovery of AGB stocks in other land cover types, principally rangelands (Figure
111 S2). Despite this apparent recovery of AGB stocks, the deficits in these regions were still >50 Mg C
112 ha^{-1} in 2012.

113 Our estimates indicate a significant negative correlation between inter-annual variations of the El
114 Niño/Southern Oscillation (ENSO), represented by a winter composite of the Multivariate ENSO
115 Index (MEI_w, see methods) and detrended ΔAGB_{pot} integrated over previously disturbed regions

(Figure S3 in the Supplementary Information; $r = -0.57$; $p \approx 0.01$). This relationship indicates that negative (La Niña) phases of ENSO would drive positive anomalies in ΔAGB_{pot}, i.e. a stronger sink, while positive (El Niño) phases of ENSO are associated with negative anomalies in ΔAGB_{pot}, a weaker sink. However, past and current human activities mean that this significant relationship between ENSO and the sink strength disappears when comparing with de-trended ΔAGB_{obs} ($r = -0.38$, $p > 0.10$). We conclude that, through clearing and subsequent regrowth, human activities have become the main driver of inter-annual variability of the land-based sink, dominating natural climate drivers, in disturbed regions of the Amazon.

Discussion

The annual biomass maps have allowed resolution of AGB changes across the Amazon Basin, indicating areas of heavy losses, but also some areas of AGB gain (Figure 2). By mapping the potential biomass, we show the evolution of the basin's capacity to store C, a baseline without human impacts. Because AGB_{pot} is determined from annual AGB_{obs} data in IFL, the annual variation in AGB_{pot} indicates the effect of climate on the storage capacity of the intact forest. We show that this potential has declined over 1993-2012 (Figure 2) similarly to AGB stocks in IFL (Figure S4 in the Supplementary Information), due to climate and in spite of rising atmospheric CO_2 concentrations (Table 1). Indeed, the evolution of AGB stocks in IFL is significantly correlated with the vegetation water stress estimated by GLEAM[18] ($r = 0.64$; $p < 0.01$). The post-2005 decrease in AGB stocks in IFL follows a transition to stronger stress conditions around 2002 that prevail until the end of the study period in 2012. This transition toward more water-stressed conditions corresponds to the onset of the 2002-2003 El Niño episode[19] followed by the 2005 and the 2010 Amazonian droughts[20,21]. Overall, these results indicate that drying conditions have degraded the capacity of the disturbed regions to regain their lost biomass which is line with the projected risk of climate driven Amazon biomass loss[7]. This climate-driven reduction in the capacity for regeneration also corroborates with risks for tropical forests to be replaced by savannahs if drier conditions dominates[15].

Our results are first-order estimates and we are aware that hard-to-quantify and potentially large uncertainties may arise from ground-level measurements[22], the way they are used in combination with remote-sensing data to derive large-scale biomass maps[23], and the identification of forest cover[24] and intact forest landscapes[13]. Therefore, we have validated the robustness of our machine-learning approach in several ways. First, it simulates annual AGB_{obs} with <0.1% bias integrated over out-of-sample IFL regions (Figure S5a in the Supplementary Information). We note a tendency to overestimate AGB in less densely vegetated regions (Figure S5b and c in the Supplementary Information) but the local mean relative bias is <1.2%. Second, pixel to country-scale estimates of the evolution of AGB_{def} through time are in agreement with independent datasets of deforestation (Figure S1) and land cover change rates (Figure 3). Finally, the ~7.3 Pg C AGB_{def} estimated after 2005 is similar to the one reported previously[8]. Our highest confidence results indicate a ~0.08 Pg C y^{-1} increase in AGB_{def} for the period 1993-2012. This net number is about half of recent estimates of gross C emissions from the Amazonian deforestation[25]. It is in agreement with the ~50% compensation of gross C emissions from tropical deforestation by regrowth[1]. Assuming that large-scale deforestation started in 1960 (ref. 26), the initial AGB_{def} of ~5.8 Pg C in 1993 corresponds to a higher 0.18 Pg C y^{-1} net biomass loss prior to this date. The decrease in AGB_{def} growth rate between 1993 and 2012, and especially after 2005 (Figure 1), matches reports of a slowing down of Brazilian deforestation during 2005-2012 (refs. 26-28) but is also a result of a decrease in AGB_{pot} in disturbed regions of the Amazon Basin.

Furthermore, field studies[20,21] and airborne measurements[29] have shown that climate variability, and especially El Niño-induced droughts, have a large impact on the carbon balance of undisturbed areas of the Amazon Basin. These previous results are in agreement with the negative correlation between MEI_w and ΔAGB_{pot} (Figure S3 in the Supplementary Information). Overall, human-induced clearing and recovery processes mask the natural response of ecosystems to climate in disturbed parts of the Amazon Basin. While this impact is intuitive, we are able to demonstrate it quantitatively with the AGB_{pot} reconstructions. Finally, this result raises concerns on the viability of climate change mitigation strategies, as climate change is likely to challenge the resilience of forested landscapes.

Conclusion

We have recreated annual maps of potential AGB for the Amazon Basin, which allows the net impacts of global change on basin biomass to be determined. Compared to maps of historical biomass, these indicate an increase of ~1.5 Pg C in the biomass deficit (AGB_{def}) for 1993-2012. This basin-wide number is a net estimate of climate-induced variation of AGB_{pot} and deforestation-induced erosion of AGB stocks, which are partly compensated by regrowth in some areas post-deforestation. Overall, our results indicate that land use change continues to erode the carbon storage of the Amazon basin while climate change is impairing its capacity to sequester carbon through natural processes of regrowth, raising concerns on the long-term resilience of land-based mitigation strategies.

Methods

Annual maps of AGB

We use annual Above Ground Biomass maps[17] (AGB_{obs}) for the period 1993 through 2012 based on the passive microwave observed vegetation optical depth (VOD, dimensionless) from a series of satellites. VOD is an indicator of the total water content in the aboveground vegetation, i.e. including both canopy and woody components[30-32]. This VOD dataset can qualitatively capture the long-term and inter-annual variations in vegetation water content over different land cover types[33-37]. Annual AGB_{obs} maps were created by establishing a relationship between VOD and a pan-tropical map[4] of AGB_{obs} circa 2000. These annually resolved maps are comparable with previous independent estimates of AGB dynamics[1,5,6]. For more details about the methodology used to create AGB_{obs} maps, please refer to Liu et al. (2015, ref. 17).

Creating potential AGB maps

To derive the evolution of the AGB deficit (AGB_{def}) we first created annually resolved maps of potential Above Ground Biomass (AGB_{pot}) in previously disturbed regions. AGB_{pot} corresponds to AGB stocks there would exist under current climate if deforestation had not occurred in these regions. It can also be conceptualized as the current forest regeneration potential if regrowth was instantaneous. The method to create AGB_{pot} maps was described in Exbrayat and Williams (2015; ref. 8) and is only briefly summarized hereafter.

First, we used a Random Forest machine-learning algorithm[38,39] to reproduce AGB_{obs} as a function of climatology in identified Intact Forest Landscapes (IFL) which cover about 55% of the Amazon Basin. The Random Forest technique relies on multiple decision trees (here n = 1,000) to group data points as a function of driving data. Then, in each final node a multiple linear regression is trained to predict the target variable (here AGB_{obs}) as a function of explanatory data. Each individual decision tree is trained on a randomly selected subset of the data and the final prediction is the average of all trees. Here, we use the CRU CL2.0 climatology dataset[12], re-gridded to a matching 0.25° resolution

206 with the Climate Data Operators version 1.6.9, and latitude, a proxy of intra-annual photoperiod
207 amplitude, as explanatory variables to predict AGB in IFL. The assumption is made that regions
208 identified as 'intact' may be subject to small-scale indigenous management[40] or disturbances[41] that are
209 negligible at the coarser 0.25° resolution used here[8]. Compared to our previous study we used an
210 updated IFL dataset[13] that represents the extent of intact regions for the year 2013. It ensures that
211 training regions have remained intact throughout the whole period covered by the AGB_{obs} dataset (i.e.
212 1993 – 2012). In addition to these continuous drivers, we used a categorical variable to separate pixels
213 corresponding to large-scale open water regions in the Global Lakes and Wetlands Database[42]. As
214 VOD values are strongly influenced by the open water dynamics, the pixels with large-scale open
215 water are identified and the VOD values over these pixels are assumed constant among different
216 years[17].

217 Once trained the algorithm can then be used to estimate annual, climate-driven, AGB_{pot} in previously
218 disturbed regions (i.e. outside IFL) regions. Although it has been identified as the major driver of the
219 recent greening of the land surface[14], CO_2 is not explicitly used in our approach because of the lack of
220 availability of spatially-explicit data of atmospheric concentrations. However, we assume that the
221 impact of increasing CO_2 on AGB stocks is intrinsically included in time series of AGB in IFL which
222 also include the impact of changing climatic conditions. Using annual maps of AGB_{pot} we can
223 calculate an AGB deficit ($AGB_{def} = AGB_{pot} - AGB_{obs}$) and derive time series of its evolution from
224 1993 to 2012. As the temporal evolution of AGB_{pot} is only driven by climate and atmospheric CO_2
225 concentrations, we assume that AGB_{def} is representative of the net and cumulative impact of
226 anthropogenic activities on biomass dynamics on AGB stocks. We perform the analyses using the
227 mean AGB_{obs} from Liu et al. (ref. 17) to derive AGB_{pot} and AGB_{def}. Furthermore, we evaluate the
228 uncertainty in our approach by performing the analysis with the 5^{th} and 95^{th} percentiles of AGB_{obs}
229 data[17] to report the corresponding confidence ranges in AGB_{pot} and AGB_{def}. As a proof of concept, we
230 first validate the method using ~50% of randomly selected pixels in IFL as training dataset and the
231 remaining IFL pixels as target dataset to assess the robustness of the approach to recreate 20 years of
232 AGB_{pot}. Corresponding results are presented in Figure S5 of the supplement. We note a good

agreement between reconstructions and data in IFL although there is a tendency for the machine-learning to overestimate AGB in less densely vegetated regions.

Validation of results

Our estimates of AGB_{pot} cannot be directly validated against field data. However, we expect the temporal evolution of AGB_{def} to be related to contemporary deforestation rates and land cover changes. Therefore, we compare time series of AGB_{pot} from pixel to country-scale with independent datasets of Land Use and Land Cover Change (LULCC). First, we compare annual deforestation rates reported by INPE for the Brazilian part of the Amazon Basin with the corresponding trend in AGB_{def} over the whole period 1993-2012. Second, we use spatially-explicit data from the Land-Use Harmonization project version 2 (LUH2v2h; data updated from ref. 43). LUH2v2h is a global driving dataset that provides annual land cover information for the period 850-2015 C.E. in the Land Use Model Intercomparison Project[44] (LUMIP) contribution to the upcoming sixth phase of the Coupled Model Intercomparison Project[45] (CMIP6). In LUH2v2h land covers are distributed between 12 classes (2 primary land classes, 2 secondary land classes, 5 cropland classes, 2 pasture and rangeland classes and 1 urban class) and the fraction they cover in each 0.25° pixel is reported annually.

Climate sensitivity

We compare the evolution of AGB_{obs} in IFL with time series of the vegetation stress factor S from the GLEAM dataset v 3.1a (ref. 18). GLEAM is a data-assimilation system that uses satellite observations to constrain daily estimates of global terrestrial evaporation and root-zone soil moisture[46]. The factor S is an output of GLEAM and represents the ratio of actual evapotranspiration to potential evapotranspiration, an indicator of ecosystem's water stress. It is as a function of vegetation state and soil moisture availability and therefore takes long-term effects of precipitation conditions into account. We use the mean annual value of S across the IFL regions of the Amazon Basin, expressed as a z-score, to explain the evolution of AGB_{obs} (Figure S4).

We seek to further understand the impact of large-scale human disturbances by quantifying their impact on the response of ecosystems to climate variability. We focus on the El Niño/Southern Oscillation (ENSO), a main driver of global climate variability[47]. The state of ENSO, quantified through the calculations of an index, significantly correlates with the strength of the global land carbon sink[48]. Indeed, positive (negative) El Niño (La Niña) phases drive warmer and drier (cooler and wetter) conditions over large parts of the pan-tropical region, including the Amazon Basin, which explains spatial patterns of ecosystem carbon uptake[48]. Following previous studies[48,49] we use a winter composite of the Multivariate ENSO Index[50,51] calculated between Dec/Jan and Mar/Apr (referred as MEI_w). To quantify the impact of human disturbances on the response of the Amazon terrestrial carbon sink to ENSO, we study the correlation between MEI_w and detrended anomalies of annual ΔAGB_{obs} and ΔAGB_{pot} stocks integrated over disturbed (i.e. non-IFL) regions of the Amazon Basin. We choose to rely on a global index rather than actual data of temperature and precipitation for the Amazon Basin because past deforestation may have altered these quantities in regions where land-atmosphere coupling is strong[52,53].

Data availability

The data generated during this study are available from the corresponding author on reasonable request.

Acknowledgements

JFE and MW are supported by the Natural Environment Research Council through the National Centre for Earth Observation. YYL is a recipient of Thousand Talents Plan for Young Outstanding Scientists in China. The authors are grateful to the community for the availability of data and software which made this study possible:

- Climate Data Operators are available from http://www.mpimet.mpg.de/cdo
- IFL geographical data was downloaded from http://www.intactforests.org

- INPE annual estimates of Brazilian deforestation are available online at http://www.obt.inpe.br/prodes/prodes_1988_2012.htm
- LUH2 v2h data is available from http://luh.umd.edu
- Monthly MEI time series were downloaded from http://www.esrl.noaa.gov/psd/enso/mei/
- GLEAM version 3.1a is available from http://www.gleam.eu

Author contributions

All authors designed the study, YYL provided annual AGB maps, JFE performed the analyses and wrote the paper with contribution from both co-authors.

Additional information

The author(s) declare no competing financial interests.

References

1. Pan, Y. *et al.* A large and persistent carbon sink in the world's forests. *Science* **333**, 988-993 (2011).

2. Le Quéré, C. *et al.* Global Carbon Budget 2015. *Earth Syst. Sci. Data* **7**, 349-396 (2015).

3. Hansen, M. C. *et al.* High-resolution global maps of 21st-century forest cover change. *Science* **342**, 850–853 (2013).

4. Saatchi, S. S. *et al.* Benchmark map of forest carbon stocks in tropical regions across three continents. *Proc. Natl. Acad. Sci. U. S. A.* **108**, 9899–9904 (2011).

5. Baccini, A. *et al.* Estimated carbon dioxide emissions from tropical deforestation improved by carbon-density maps. *Nat. Clim. Change* **2**, 182–185 (2012).

6. Harris, N. L. *et al.* Baseline map of carbon emissions from deforestation in tropical regions. *Science* **336**, 1573–1576 (2012).

7. Cox, P. M. *et al.* Sensitivity of tropical carbon to climate change constrained by carbon dioxide variability. *Nature* **494**, 341-344 (2013).

8. Exbrayat, J.-F. & Williams, M. Quantifying the net contribution of the historical Amazonian deforestation to climate change. *Geophys. Res. Lett.* **42**, 2968–2976 (2015).

9. Friend, A. D. *et al.* Carbon residence time dominates uncertainty in terrestrial vegetation responses to future climate and atmospheric CO_2. *Proc. Natl. Acad. Sci. U. S. A.* **111**, 3280–3285 (2014).

10. Nishina, K. *et al.* Quantifying uncertainties in soil carbon responses to changes in global mean temperature and precipitation. *Earth Syst. Dyn.* **5**, 197–209 (2014).

11. Warszawski, L. *et al.* The Inter-Sectoral Impact Model Intercomparison Project (ISI-MIP): project framework. *Proc. Natl. Acad. Sci. U. S. A.* **111**, 3228–32 (2014).

12. New, M., Lister D., Hulme M. & Makin, I. A high-resolution data set of surface climate over global land areas. *Clim. Res.* **21**, 1–25 (2002).

13. Potapov, P. *et al.* Mapping the world's intact forest landscapes by remote sensing. *Ecol. Soc.* **13**, doi:Artn 51, (2008).

14. Zhu, Z. *et al.* Greening of the Earth and its drivers. *Nat. Clim. Change* **6**, 791-795 (2016).

15. M. Hirota, Holmgren, M., Van Nes, E. H. & Scheffer M. Global resilience of tropical forest and savanna to critical transitions. *Science* **334**, 232–235 (2011).

16. Rammig, A. *et al.* Estimating the risk of Amazonian forest dieback. *New Phytol.* **187**, 694–706 (2010).

17. Liu, Y. Y. *et al.* Recent reversal in loss of global terrestrial biomass. *Nat. Clim. Change* **5**, 470–474 (2015).

18. Martens *et al.* GLEAM v3: satellite-based land evaporation and root-zone soil moisture. *Geosci. Model Dev.* **10**, 1903-1925 (2017).

19. Zeng *et al.* Causes and impacts of the 2005 Amazon drought. *Env. Res. Lett.* **3**, 014002 (2008).

20. Phillips, O. L. *et al.* Drought sensitivity of the Amazon rainforest. *Science* **323**, 1344-1347 (2009).

21. Lewis, S. L. *et al.* The 2010 Amazon drought. *Science* **331**, 554 (2011).

22. Chave, J. *et al.* Improved allometric models to estimate the aboveground biomass of tropical trees. *Glob. Chang. Biol.* **20**, 3177–3190 (2014).

23. Réjou-Méchain, M. *et al.* Local spatial structure of forest biomass and its consequences for remote sensing of carbon stocks. *Biogeosciences* **11**, 5711– 5742 (2014).

24. Sexton, J. O. *et al.* Conservation policy and the measurement of forests. *Nat. Clim. Chang.* **6**, 192–196 (2015).

343 25. Loarie, S. R., Asner, G. P. & Field, C. B. Boosted carbon emissions from Amazon deforestation.
344 *Geophys. Res. Lett.* **36**, L14810 (2009).

345 26. Ramankutty, N. *et al.* Challenges to estimating carbon emissions from tropical deforestation.
346 *Global Change Biol.* **13**, 51–66 (2007).

347 27. Nepstad, D. *et al.* Inhibition of Amazon deforestation and fire by parks and indigenous lands.
348 *Conservat. Biol.* **20**, 65–73 (2006).

349 28. Malhi, Y. *et al.* Climate change, deforestation, and the fate of the Amazon. *Science* **319**, 169–72
350 (2008).

351 29. Gatti, L. V. *et al.* Drought sensitivity of Amazonian carbon balance revealed by atmospheric
352 measurements. *Nature* **506**, 76-80 (2014).

353 30. Jackson, T. J. & Schmugge, T. J. Vegetation effects on the microwave emission of soils. *Remote*
354 *Sens. Environ.* **36**, 203–212 (1991).

355 31. Kerr, Y. H. & Njoku, E. G. A semiempirical model for interpreting microwave emission from
356 semiarid land surfaces as seen from space. *IEEE Trans. Geosci. Remote Sensing* **28**, 384–393
357 (1990).

358 32. Guglielmetti, M. *et al.* Measured microwave radiative transfer properties of a deciduous forest
359 canopy. *Remote Sens. Environ.* **109**, 523–532 (2007).

360 33. Liu, Y. Y., de Jeu, R. A. M., McCabe, M. F., Evans, J. P. & van Dijk, A. I. J. M. Global long-
361 termpassive microwave satellite-based retrievals of vegetation optical depth. *Geophys. Res.*
362 *Lett.* **38**, L18402 (2011).

363 34. Liu, Y. Y., van Dijk, A. I. J. M., McCabe, M. F., Evans, J. P. & de Jeu, R. A. M. Global
364 vegetation biomass change (1988–2008) and attribution to environmental and human drivers.
365 *Glob. Ecol. Biogeogr.* **22**, 692–705 (2013).

35. Andela, N., Liu, Y. Y., van Dijk, A. I. J. M., de Jeu R. A. M. & McVicar T. R. Global changes in dryland vegetation dynamics (1988-2008) assessed by satellite remote sensing: comparing a new passive microwave vegetation density record with reflective greenness data. *Biogeosciences* **10**, 6657-6676 (2013).

36. Tian, F. *et al.* Remote sensing of vegetation dynamics in drylands: Evaluating vegetation optical depth (VOD) using AVHRR NDVI and in situ green biomass data over West African Sahel. *Remote Sens. Environ.* **177**, 265-276 (2016).

37. Tian, F., Brandt, M., Liu, Y. Y., Rasmussen, K., & Fensholt, R. Mapping gains and losses in woody vegetation across global tropical drylands. *Glob. Change Biol.* **23**, 1748-1760 (2017).

38. Breiman, L. Random forests. *Mach. Learn.* **45**, 5–32 (2001).

39. Pedregosa, F. *et al.* Scikit-learn: Machine Learning in Python. *J. Mach. Learn. Res.* **12**, 2825–2830 (2011).

40. Ramankutty, N. & Foley, J. A. Estimating historical changes in global land cover: Croplands from 1700 to 1992. *Glob. Biogeochem. Cycles* **13**, 997–1027 (1999).

41. Espírito-Santo, F. D. B. B. *et al.* Size and frequency of natural forest disturbances and the Amazon forest carbon balance. *Nat. Commun.* **5**, 3434; 10.1038/ncomms4434 (2014).

42. Lehner, B. & Doll, P. Development and Validation of a Global Database of Lakes, Reservoirs and Wetlands. *J. Hydrol.* **296**, 1–22 (2004).

43. Hurtt, G. C. *et al.* Harmonization of land-use scenarios for the period 1500–2100: 600 years of global gridded annual land-use transitions, wood harvest, and resulting secondary lands. *Climatic Change* **109**, 117–161 (2011).

44. Lawrence, D. M. *et al.* The Land Use Model Intercomparison Project (LUMIP) contribution to CMIP6: rationale and experimental design. *Geosci. Model Dev.* **9**, 2973-2998 (2016).

389 45. Eyring, V. *et al.* Overview of the Coupled Model Intercomparison Project Phase 6 (CMIP6)
390 experimental design and organization. *Geosci. Model Dev.* **9**, 1937-1958 (2016).

391 46. Miralles, D.G. *et al.* Global land-surface evaporation estimated from satellite-based observations,
392 *Hydrol. Earth Syst.Sci.* **15**, 453–469 (2011).

393 47. Trenberth, K. The Definition of El Niño. *Bull. Amer. Meteor. Soc.* **78**, 2771–2777 (1997).

394 48. Bastos, A., Running, S. W., Gouveia, C. & Trigo, R. M. The global NPP dependence on ENSO:
395 La Niña and the extraordinary year of 2011. *J. Geophys. Res. Biogeosciences* **118**, 1247-1255
396 (2013).

397 49. Vicente-Serrano, S. M. *et al.* A multiscalar global evaluation of the impact of ENSO on droughts.
398 *J. Geophys. Res. Atmospheres* **116**, D20109 (2011).

399 50. Wolter, K. & Timlin, M. S. Measuring the strength of ENSO events - how does 1997/98 rank?
400 *Weather* **53**, 315-324 (1998).

401 51. Wolter, K. & Timlin, M. S. El Niño/Southern Oscillation behaviour since 1871 as diagnosed in an
402 extended multivariate ENSO index (MEI.ext). *Intl. J. Climatology* **31**, 1074-1087 (2011).

403 52. Koster, R. D. *et al.* Regions of strong coupling between soil moisture and precipitation. *Science*
404 **305**, 1138–1140 (2004).

405 53. Lorenz, R. & Pitman, A. J. Effect of land-atmosphere coupling strength on impacts from
406 Amazonian deforestation. *Geophys. Res. Lett.* **41**, 5987–5995 (2014).

407

Tables

Table 1. Total AGB_{obs} in the disturbed regions of the Amazon Basin from Liu et al. (2015) and AGB_{pot} from this study in 1993 and 2012. Reported values are mean, with 5th and 95th percentiles between brackets. All values are in Pg C, rounded to the first decimal.

1993			2012		
AGB_{obs}	AGB_{pot}	AGB_{def}/AGB_{pot}	AGB_{obs}	AGB_{pot}	AGB_{def}/AGB_{pot}
26.3 (24.0 / 28.1)	32.1 (29.8 / 33.8)	18.0% (17.0% / 19.3%)	24.1 (22.0 / 25.9)	31.4 (29.2 / 33.1)	23.3% (22.0% / 24.7%)

Figures

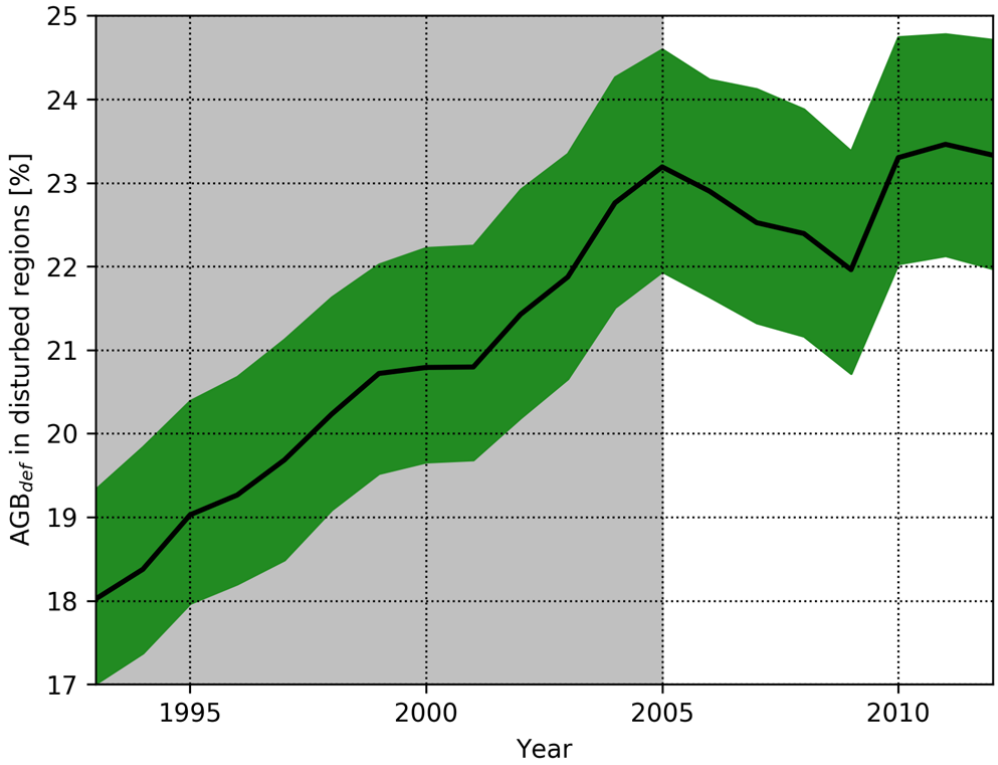

Figure 1. Time series of AGB_{def} in disturbed areas of the Amazon Basin expressed as a fraction of AGB_{pot}. The green area represents the 5^{th} and 95^{th} percentile while the thick black line represents the mean. The shaded time period 1993-2005 highlights when the basin-wide increase in AGB_{def} exhibits a linear trend ($r = 0.99$; $p << 0.001$) before this trend disappears after 2005.

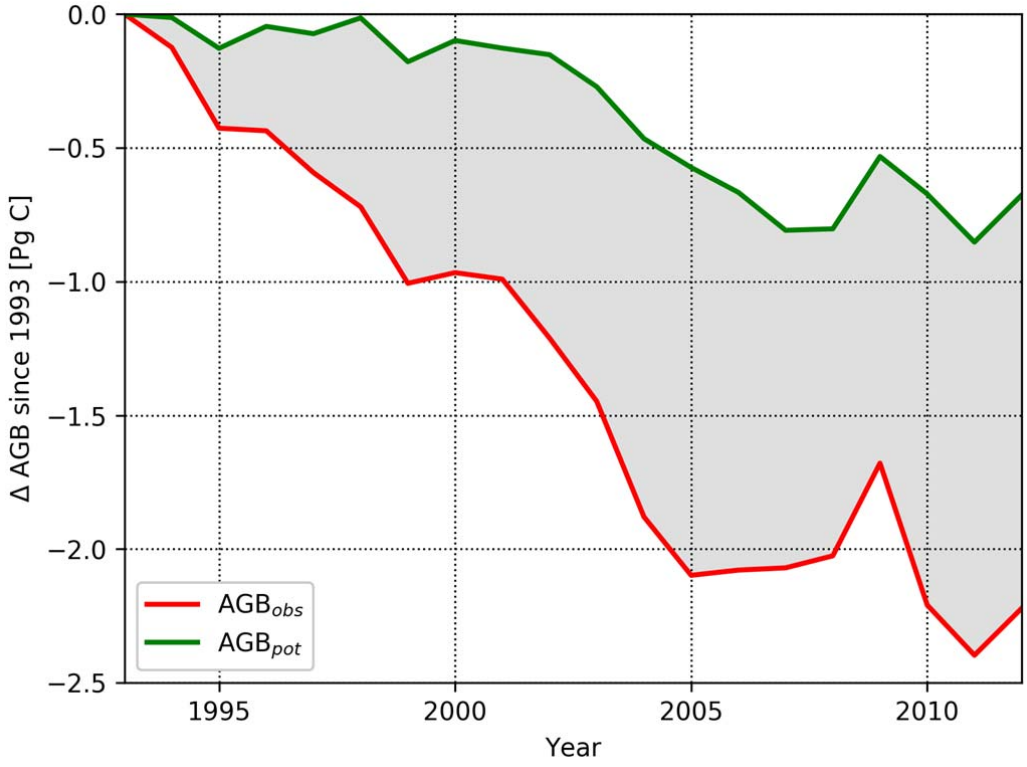

Figure 2. Change in total AGB_{obs} and AGB_{pot} in previously disturbed regions since 1993. Differences between AGB_{pot} and AGB_{obs}, represented as a grey shading, correspond to the evolution of AGB_{def} for 1993-2012. For clarity only the mean estimates are represented.

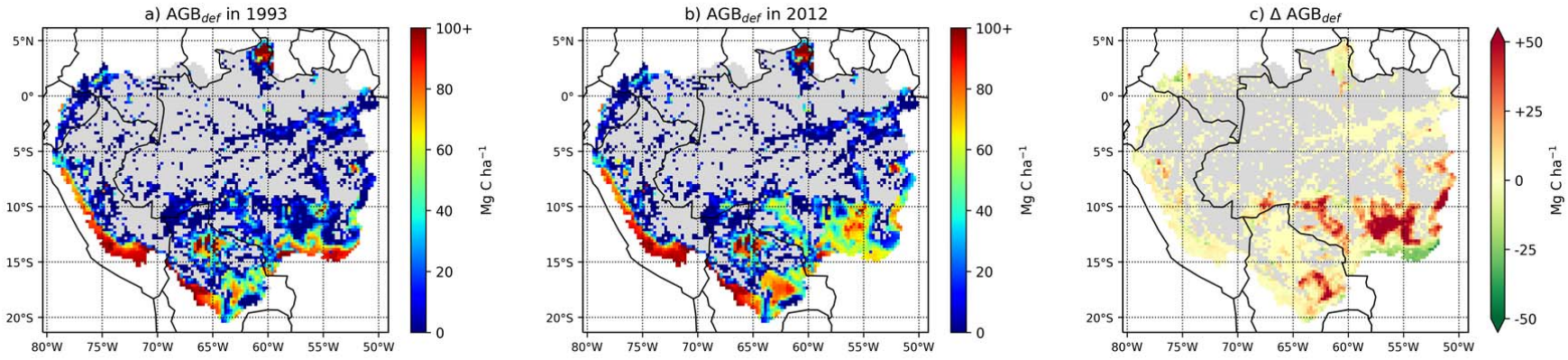

Figure 3. Aboveground Biomass Carbon deficit (AGB_{def}) in (a) 1993, (b) 2012 and (c) the change in AGB_{def} over these two decades (c). Untouched IFL areas are represented in grey. In sub-panel c, positive (red) values indicate an erosion of AGB stocks while negative (green) values indicate a partial recovery. Maps were created using the cartopy module version 0.12.0 (http://scitools.org.uk/cartopy/) for python 2.7 (http://www.python.org/).

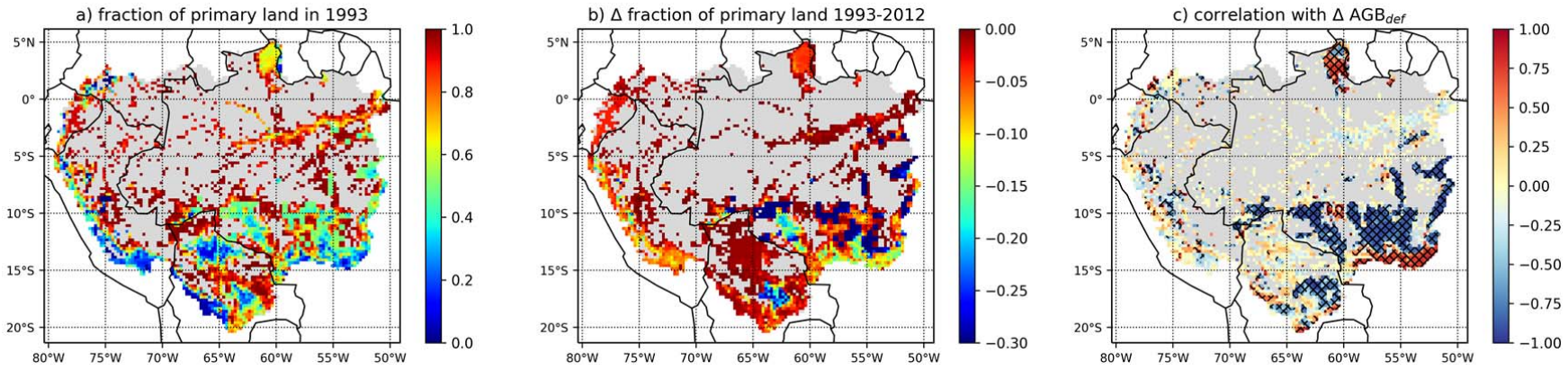

Figure 4. (a) Fraction of primary land outside IFL regions in 1993. Grey areas represent IFL regions. (b) Change in fraction of primary land between 1993 and 2012. Blue represents the decline in primary land during 1993-2012. (c) Temporal correlation between fraction of primary land and AGB_{def} from 1993 through 2012 over each 0.25° grid cell. Hatched areas represent statistically significant correlation ($p < 0.05$). A negative correlation indicates an increase in AGB_{def} (i.e. an erosion of AGB stocks) when the fraction of primary land decreases through time. Maps were created using the cartopy module version 0.12.0 (http://scitools.org.uk/cartopy/) for python 2.7 (http://www.python.org/).